Back to Session Subjects

NONLINEAR ANALYSIS OF A SUPERCRITICAL HELICOPTER'S TAIL ROTOR DRIVE SHAFT FLEXURAL VIBRATIONS

Zbigniew Dżygadło and Witold Perkowski
Institute of Aviation, Al. Krakowska 110/114
02-256 Warsaw, Poland

Abstract

In the new ultra-light helicopter, just now designed in the Institute of Aviation, a light-weight supercritical tail rotor drive shaft will be used. This paper presents a nonlinear dynamic model of such a shaft for the analysis of its flexural vibrations.

The model assumes that the shaft has several deformable supports with elastic and damping elements and is loaded by external forces caused by its local unbalance.

The equations of motion have been obtained making use of the finite element method and dividing the shaft into several elements between successive supports.

In order to ensure easy crossing through a resonance region, a nonlinear dry friction damper has been applied in the shaft structure. Depending on the parameters of this damper, we can obtain various bending vibrations of the shaft under consideration. There can be regular or chaotic vibrations of the shaft.

1. Introduction

The dynamics of a supercritical tail rotor drive shaft is an interesting nonlinear problem of easy crossing through a resonance region [1]-[6].

The dynamic model considered in this paper assumes that the shaft is a continuous structure having several deformable supports with elastic and damping elements and is loaded by external forces caused by its local unbalance [1]-[3], [6].

The equations of motion have been determined by making use of the finite element method. Displacements of elements axes have been obtained by means of Hermite's polynomials and elements with four degrees of freedom have been determined in every of both considered planes [6].

Equations of motion of particular elements obtained from the virtual work principle, have been transformed into complex form and matrix equation of the whole shaft structure has been obtained including shaft supports.

A nonlinear dry friction damper has been applied in the shaft structure to ensure easy crossing through the resonance region. Depending on the parameters of the damper, various bending vibrations of the shaft can be obtained, which can be regular or chaotic ones [4], [5].

2. Equations of the Problem

Let us consider a supercritical tail rotor drive shaft moving with variable angular speed Ω and composed of a structure with continuous mass and elasticity distribution, having several deformable supports with elastic and damping elements and loaded by external forces caused by its local unbalance (Fig.1).

The equations of shaft motion can be obtained in a fixed orthogonal system of coordinates *0xyz* where the *x*-axis determines the position of a non-deformable shaft axis.

The equations of shaft motions will be developed making use of the finite element method and Hermite's polynomials for describing displacements of an element axis.

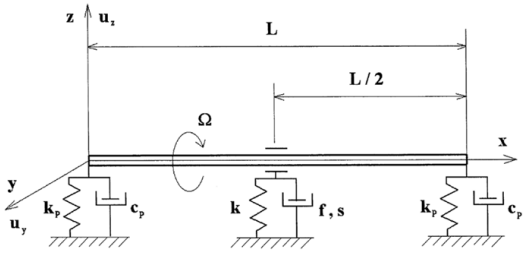

Fig.1. Sketch of the shaft.

By way of example we can show the equations of motion for a *j*-finite element

$$\begin{aligned}\mathbf{B}_j\ddot{\boldsymbol{\delta}}_{yj}+\mathbf{c}_j\dot{\boldsymbol{\delta}}_{yj}+\Omega\mathbf{I}_{oj}\dot{\boldsymbol{\delta}}_{zj}+\mathbf{K}_j\boldsymbol{\delta}_{yj}&=\mathbf{F}_{eyj}+\mathbf{F}_{exyj}\\ \mathbf{B}_j\ddot{\boldsymbol{\delta}}_{zj}+\mathbf{c}_j\dot{\boldsymbol{\delta}}_{zj}-\Omega\mathbf{I}_{oj}\dot{\boldsymbol{\delta}}_{yj}+\mathbf{K}_j\boldsymbol{\delta}_{zj}&=\mathbf{F}_{ezj}+\mathbf{F}_{exzj}\end{aligned} \tag{1}$$

where

$$\begin{aligned}\boldsymbol{\delta}_{yj}&=\boldsymbol{\delta}_{yj}(t)=\left(u_{yj-1},\theta_{yj-1},u_{yj},\theta_{yj}\right)^T\\ \boldsymbol{\delta}_{zj}&=\boldsymbol{\delta}_{zj}(t)=\left(u_{zj-1},\theta_{zj-1},u_{zj},\theta_{zj}\right)^T\end{aligned} \tag{2}$$

are examples of the displacement vectors of *j*-finite element in the *yx* and *zx* planes, and $u_{yj-1}, u_{yj}, u_{zj-1}, u_{zj}$ are dimensionless displacements, which are referred to *L*-length of the shaft, while $\theta_{yj-1}, \theta_{yj}, \theta_{zj-1}, \theta_{zj}$ are angles of rotations of both edges of j-finite element in *yx* and *zx* planes.

$\mathbf{B}_j=\mathbf{m}_j+\mathbf{I}_{1j}$; $\mathbf{I}_{oj}$ are inertial matrices,

$\mathbf{c}_j$ is external damping matrix

$\mathbf{K}_j$ is stiffness matrix,

$\mathbf{F}_{eyj}, \mathbf{F}_{ezj}$ are edge forces vectors and

$$\mathbf{F}_{exyj} = \mathbf{P}_{oj}\left[\Omega^2\cos(\Omega t)+\frac{d\Omega}{dt}\sin(\Omega t)\right]$$
$$\mathbf{F}_{exzj} = \mathbf{P}_{oj}\left[\Omega^2\sin(\Omega t)-\frac{d\Omega}{dt}\cos(\Omega t)\right] \quad (3)$$

are external, unbalance forces vectors, $\mathbf{P_{oj}}$ is vector of the amplitude of unbalance forces.

If we introduce a complex vector of the element displacements

$$\begin{aligned}\boldsymbol{\delta}_{cj} &= \boldsymbol{\delta}_{yj} + i\boldsymbol{\delta}_{zj}\\ u_{cj} &= u_{yj} + iu_{zj}\\ \theta_{cj} &= \theta_{yj} + i\theta_{zj}\end{aligned} \quad (4)$$

Eqs. (1) can be presented in the complex form

$$\mathbf{B}_j\ddot{\boldsymbol{\delta}}_{cj} + \left(\mathbf{c}_j - i\Omega\mathbf{I}_{oj}\right)\dot{\boldsymbol{\delta}}_{cj} + \mathbf{K}_j\boldsymbol{\delta}_{cj} = \mathbf{F}_{ecj} + \mathbf{F}_{excj} \quad (5)$$

where

$$\mathbf{F}_{ecj} = \mathbf{F}_{eyj} + i\mathbf{F}_{ezj} \quad (6)$$

$$\mathbf{F}_{excj} = \mathbf{P}_{oj}\left(\Omega^2 - i\frac{d\Omega}{dt}\right)e^{i\Omega t} \quad (7)$$

If we make the sum by adding together Eqs. (1) or (5) for $j = 1,2,..,n$, where n is the number of finite elements into which the shaft is divided, we obtain the matrix equations of the whole shaft structure.

$$\begin{aligned}\mathbf{B}\ddot{\boldsymbol{\delta}}_y + \mathbf{c}\dot{\boldsymbol{\delta}}_y + \Omega\mathbf{I}_o\dot{\boldsymbol{\delta}}_z + \mathbf{K}\boldsymbol{\delta}_y &= \mathbf{F}_{ey} + \mathbf{F}_{exy}\\ \mathbf{B}\ddot{\boldsymbol{\delta}}_z + \mathbf{c}\dot{\boldsymbol{\delta}}_z - \Omega\mathbf{I}_o\dot{\boldsymbol{\delta}}_y + \mathbf{K}\boldsymbol{\delta}_z &= \mathbf{F}_{ez} + \mathbf{F}_{exz}\end{aligned} \quad (8)$$

or in the complex form

$$\begin{aligned}&\mathbf{B}\ddot{\boldsymbol{\delta}}_c + \left(\mathbf{c} - i\Omega\mathbf{I}_o\right)\dot{\boldsymbol{\delta}}_c + \mathbf{K}\boldsymbol{\delta}_c =\\ &= \mathbf{F}_{ec} + \mathbf{P}_o\left(\Omega^2 - i\frac{d\Omega}{dt}\right)e^{i\Omega t}\end{aligned} \quad (9)$$

Equations (8) or (9) enable us to study the dynamics of shaft rotation with variable angular velocity Ω and to determine a method of easy crossing through a resonance region.

3. Dry Friction Damper

A nonlinear dry friction damper has been applied in the tail rotor drive shaft structure in order to ensure easy crossing through the resonance region. Its sketch is presented in Fig. 2.

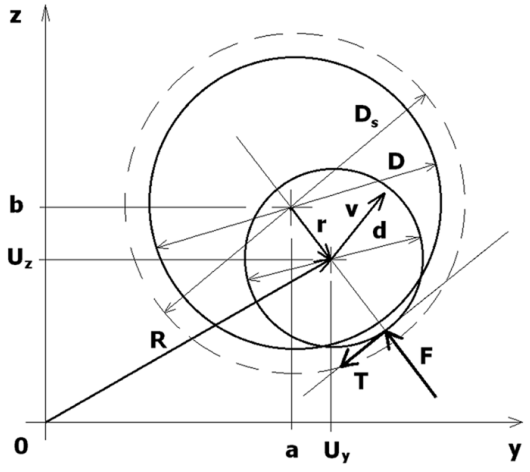

Fig.2. Sketch of the damper.

A disk with a central hole of D-diameter is the essential part of the damper. The disk is located in a housing, which causes a dry friction on both sides of the disk by means of the controlled press. It results in a resisting force *f* of the damper.

The shaft passes through the central hole of the damper and there is a gap between the hole and the shaft

$$s = 0.5(D - d) \quad (10)$$

where *d* is the shaft diameter.

The shaft can move the damper disk in the *yz*-plane after overcoming the resistance force *f*. The radial force *F* of interaction between the shaft and the damper is acting along the line connecting their centers (Fig. 2). The tangent force *T* of interaction is perpendicular to force *F* and is defined as :

$$T = F \cdot \mu \quad (11)$$

where μ is the coefficient of tangent friction.

The mass of the damper disk is neglected.

It is assumed that the damper disk has an elastic zone of D_s diameter in which the force *F* is varying from zero to *f* (Fig.3).

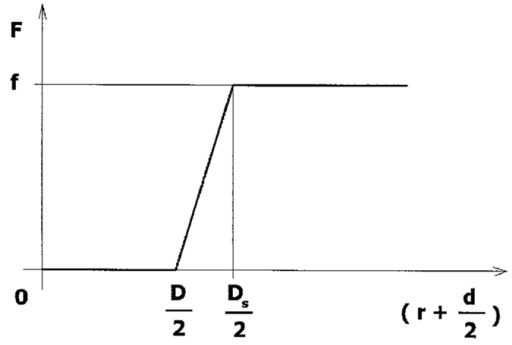

Fig.3. The radial force *F* of interaction.

The damper disk can move together with the shaft under its pressure when the force F has its maximal value.

The characteristic parameters of the damper are :

f	maximal force,
$s = (D - d)/2$	gap,
$h = (D_s - D)/2$	width of elastic zone,
$a(0)$, $b(0)$	initial position,
μ	coefficient of tangent friction.

The mathematical model of the damper is the following :

1) Components of force F :

for $r + \frac{d}{2} > \frac{D_s}{2}$:

$$\begin{cases} F_y = -f\dfrac{U_y - a}{r} \\ F_z = -f\dfrac{U_z - b}{r} \\ a_t = a_{t-1} + \dfrac{1}{2}(2r + d - D_s)\dfrac{U_y - a_{t-1}}{r} \\ b_t = b_{t-1} + \dfrac{1}{2}(2r + d - D_s)\dfrac{U_z - b_{t-1}}{r} \end{cases} \quad (12)$$

for $\frac{D}{2} \le r + \frac{d}{2} \le \frac{D_s}{2}$:

$$\begin{cases} F_y = -f\,\dfrac{(U_y - a)(2r + d - D)}{r(D_s - D)} \\ F_z = -f\,\dfrac{(U_z - b)(2r + d - D)}{r(D_s - D)} \end{cases} \tag{13}$$

for $r + \frac{d}{2} < \frac{D}{2}$:

$$\begin{cases} F_y = 0 \\ F_z = 0 \end{cases} \tag{14}$$

where :

$$r = \sqrt{(U_y - a)^2 + (U_z - b)^2} \tag{15}$$

$$R = \sqrt{U_y^2 + U_z^2} \tag{16}$$

U_y , U_z are dimensional displacements of the shaft.

2) Components of force T :

$$\begin{cases} T_y = \mu \cdot F_z \\ T_z = -\mu \cdot F_y \end{cases} \tag{17}$$

or

$$\begin{cases} T_y = -\mu \cdot F_z \\ T_z = \mu \cdot F_y \end{cases} \tag{18}$$

depend on force F and sense of vector of the shaft velocity v (fig.2). There should be an obtuse angle between vectors T and v :

$$\vec{T} \cdot \vec{v} < 0 \tag{19}$$

Forces F and T are introduced into Eqs. (8), (9) as additional edge forces.

4. Simulation of the crossing through the resonance region

The crossing through the resonance region is investigated under assumption that the shaft is homogeneous and has the following parameters :

L = 3.32 m length,
ρ = 2700 kg/m^3 density,
A = 0.00022 m^2 cross-sectional area,
$E = 0.7 \cdot 10^{11}$ Pa Young modulus,
$I = 59.3 \cdot 10^{-9}$ m^4 moment of inertia,
e = 0.001 m mass excentrity,
c = 0.5 Ns/m external damping,
$k_p = 10^6$ N/m rigidity of supports,
c_p = 0 Ns/m damping in the supports.

The shaft is divided into four finite elements of the same length. Equations of motion (8) have been solved by means of the Runge-Kutta method.
In order to present the damper parameters and results of computation in a dimensionless form an approximated mass m_0 and rigidity k_0 of the shaft have been determined making use of Rayleigh method :

$$m_0 \approx 0.5\rho AL \;;\; k_0 = \frac{48EJ}{L^3} \tag{20}$$

It results that the first frequency of the shaft is:

$$\Omega_0 = \sqrt{\frac{k_0}{m_0}} \approx 74\ rad/s\ . \tag{21}$$

Dimensionless parameters of the damper are:

$$f^* = \frac{f}{m_0 \Omega_0^2 e} \;;\; s^* = \frac{s}{e} \;;\; h^* = \frac{h}{e}. \tag{22}$$

Calculations have been performed for the one variant of the gap : s^* = 3, and for three variants of coefficient of tangent friction : μ = 0 ; 0.2 ; 0.8.
It has been also assumed that:

$a(0) = b(0) = 0$; h^*= 0.2= const. (23)

Displacements of the shaft have been analyzed for the point located in the center o the shaft (x/L = 0.5). The damper was located in the same point (Fig.1). The velocity of rotation of the shaft was assumed as:

$$\Omega(t) = \Omega(0) + \varepsilon t = 10t\ . \tag{24}$$

Results of calculations have been presented in the form of dimensionless displacement R/e depending on dimensionless velocity of rotation Ω/Ω_0 for variable parameters: f^* , μ. Results are presented in the next Figures.
In Fig.4 we can see the vibrations of the shaft without damper ($s^* = f^* = h^* = \mu = 0$).

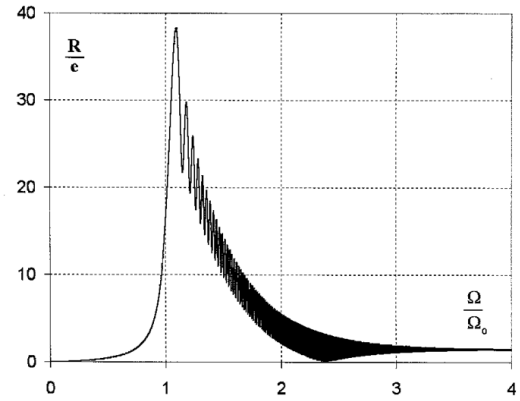

Fig.4 $s^* = 0$; $f^* = 0$; $h^* = 0$; $\mu = 0$.

In the Figs. 5 to 12 we can see vibrations of the shaft with the damper for: $s^* = 3$, $h^* = 0.2$, $\mu = 0$ and variable f^*.

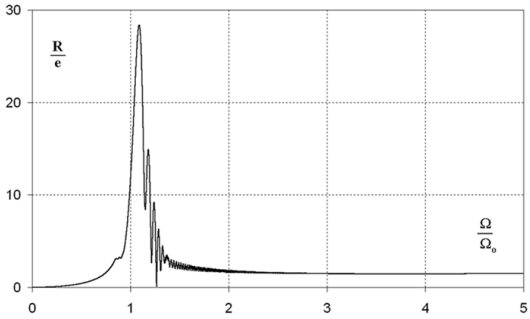

Fig.5 $s^* = 3$; $f^* = 0.183$; $h^* = 0.2$; $\mu = 0$.

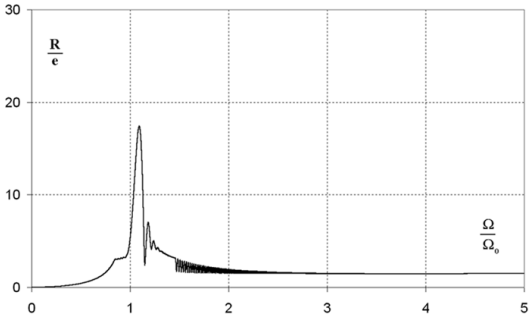

Fig.6 $s^* = 3$; $f^* = 0.366$; $h^* = 0.2$; $\mu = 0$.

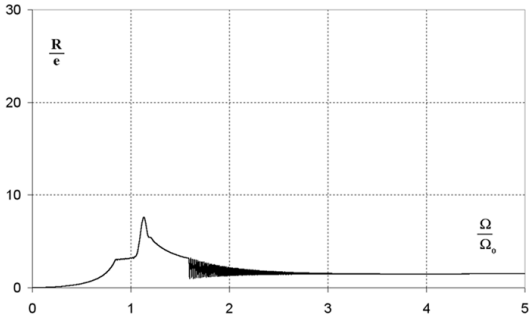

Fig.7 $s^* = 3$; $f^* = 0.732$; $h^* = 0.2$; $\mu = 0$.

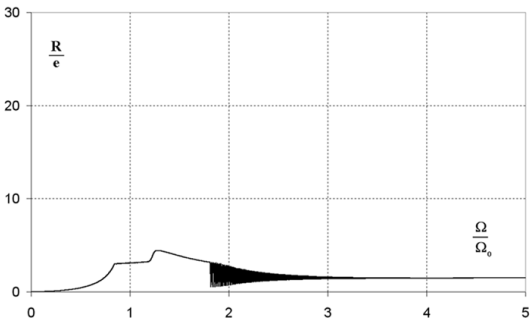

Fig.8 $s^* = 3$; $f^* = 1.464$; $h^* = 0.2$; $\mu = 0$.

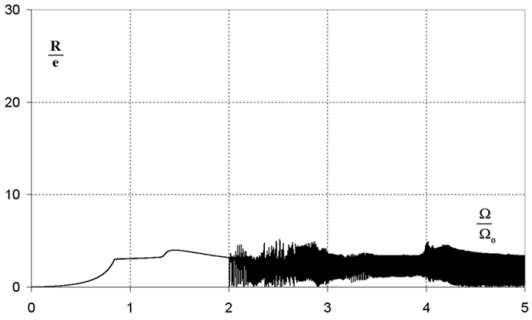

Fig.9 $s^* = 3$; $f^* = 2.196$; $h^* = 0.2$; $\mu = 0$.

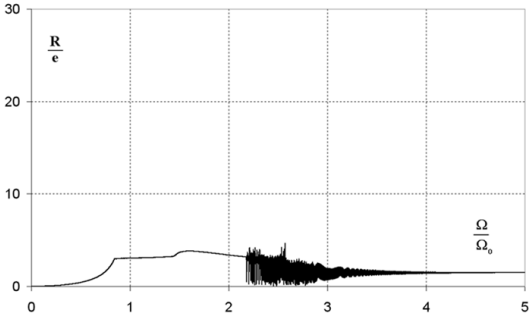

Fig.10 $s^* = 3$; $f^* = 2.928$; $h^* = 0.2$; $\mu = 0$.

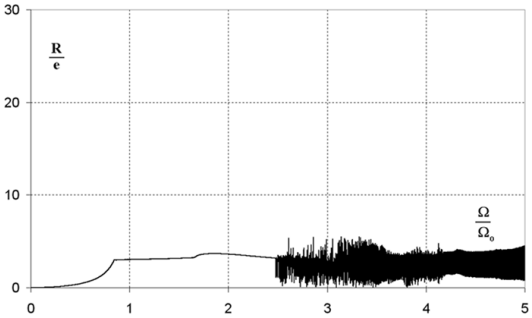

Fig.11 $s^* = 3$; $f^* = 4.392$; $h^* = 0.2$; $\mu = 0$.

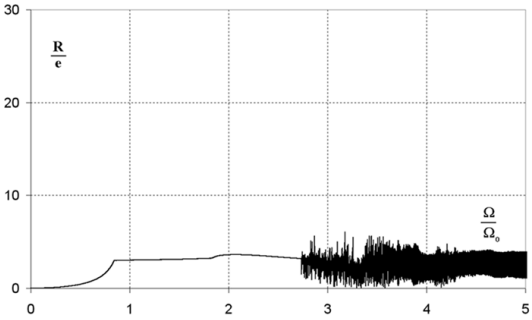

Fig.12 $s^* = 3$; $f^* = 5.856$; $h^* = 0.2$; $\mu = 0$.

In the next Figs. 13 to 20 we see the course of vibrations for the shaft with the damper for: $s^* = 3$, $h^* = 0.2$, $\mu = 0.2$ and variable f^*.

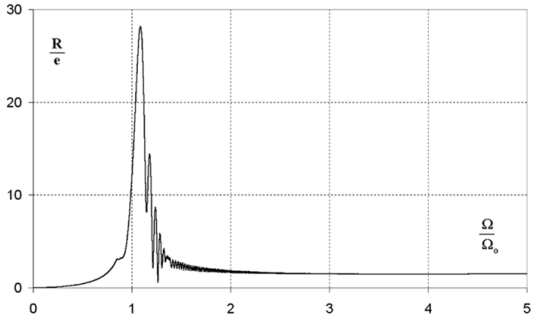

Fig.13 $s^* = 3$; $f^* = 0.183$; $h^* = 0.2$; $\mu = 0.2$.

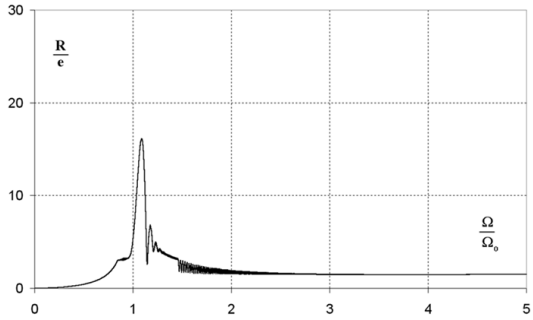

Fig.14 $s^* = 3$; $f^* = 0.366$; $h^* = 0.2$; $\mu = 0.2$.

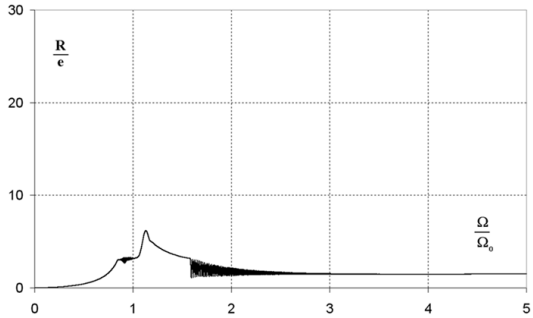

Fig.15 $s^* = 3$; $f^* = 0.732$; $h^* = 0.2$; $\mu = 0.2$.

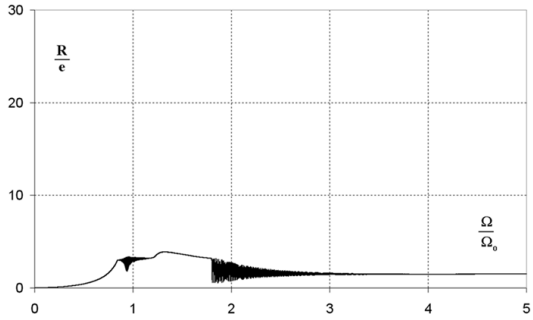

Fig.16 $s^* = 3$; $f^* = 1.464$; $h^* = 0.2$; $\mu = 0.2$.

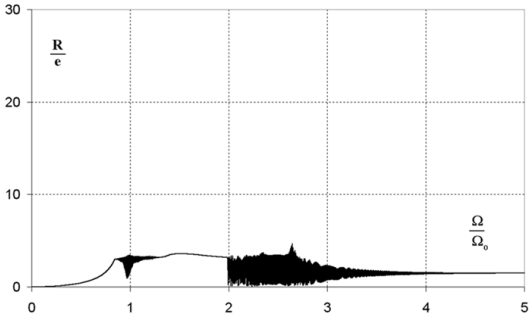

Fig.17 $s^* = 3$; $f^* = 2.196$; $h^* = 0.2$; $\mu = 0.2$.

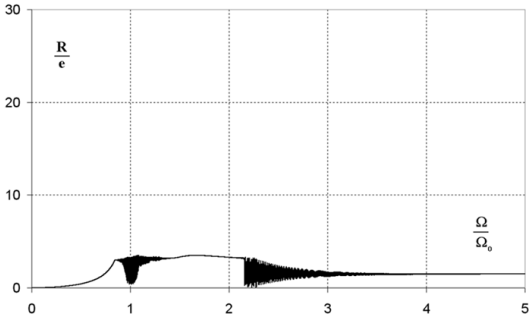

Fig.18 $s^* = 3$; $f^* = 2.928$; $h^* = 0.2$; $\mu = 0.2$.

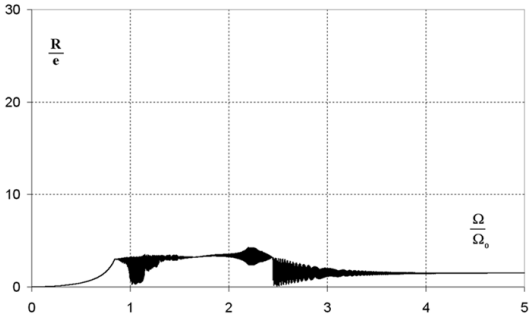

Fig.19 $s^* = 3$; $f^* = 4.392$; $h^* = 0.2$; $\mu = 0.2$.

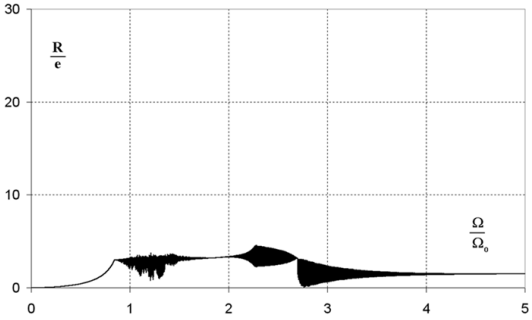

Fig.20 $s^* = 3$; $f^* = 5.856$; $h^* = 0.2$; $\mu = 0.2$.

In the Figs. 21 to 28 the shaft vibrations are presented for: $s^* = 3$, $h^* = 0.2$, $\mu = 0.8$ and variable f^*.

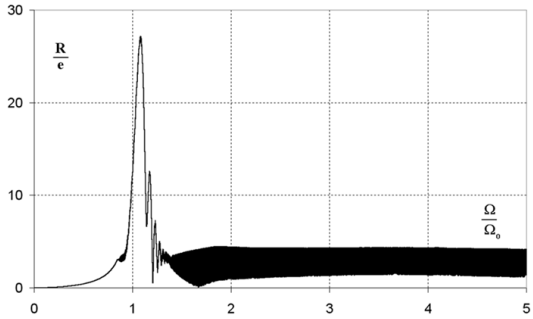

Fig.21 $s^* = 3$; $f^* = 0.183$; $h^* = 0.2$; $\mu = 0.8$.

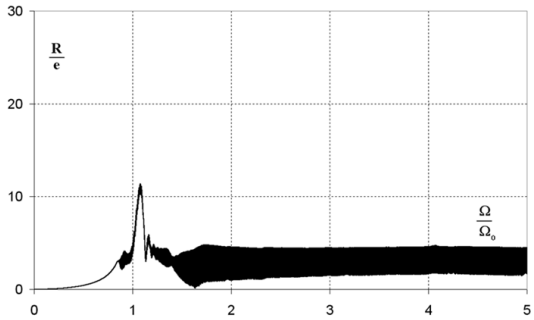

Fig.22 $s^* = 3$; $f^* = 0.366$; $h^* = 0.2$; $\mu = 0.8$.

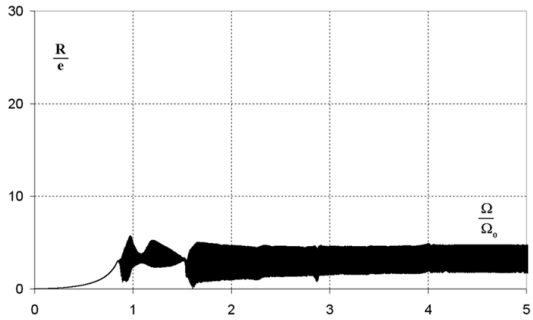

Fig.23 $s^* = 3$; $f^* = 0.732$; $h^* = 0.2$; $\mu = 0.8$.

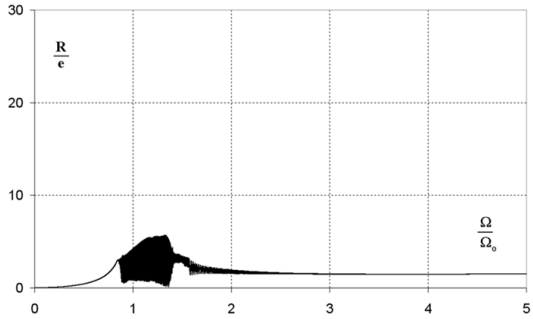

Fig.24 $s^* = 3$; $f^* = 1.464$; $h^* = 0.2$; $\mu = 0.8$.

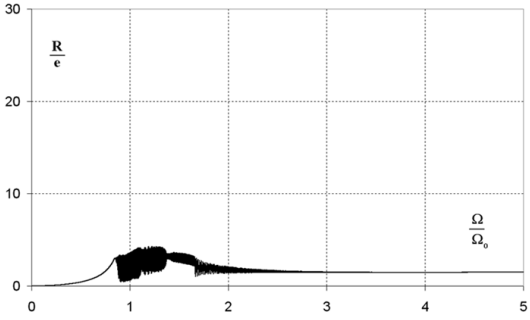

Fig.25 $s^* = 3$; $f^* = 2.196$; $h^* = 0.2$; $\mu = 0.8$.

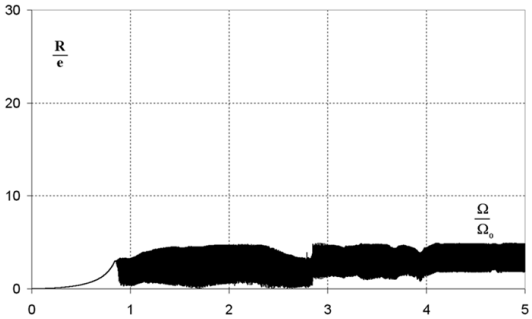

Fig.26 $s^* = 3$; $f^* = 2.928$; $h^* = 0.2$; $\mu = 0.8$.

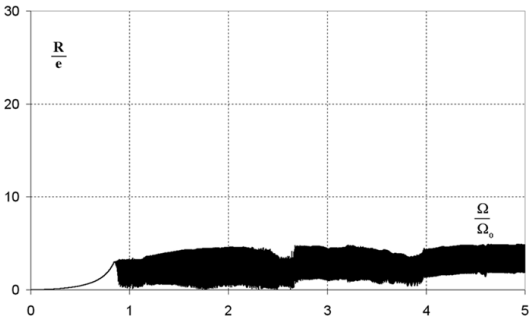

Fig.27 $s^* = 3$; $f^* = 4.392$; $h^* = 0.2$; $\mu = 0.8$.

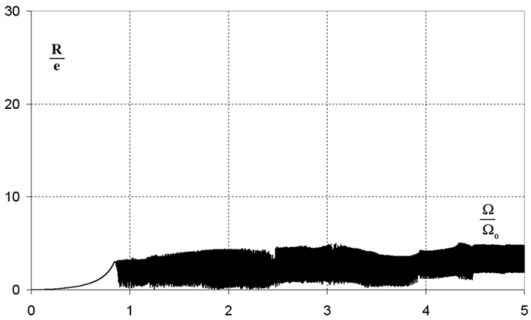

Fig.28 $s^* = 3$; $f^* = 5.856$; $h^* = 0.2$; $\mu = 0.8$.

In the figures 5-12 (damper without tangent friction) we can see that shaft cannot loose contact with the damper if force f^* is too high. For example there are irregular vibrations visible in Fig.9. The course of these vibrations is shown in Figs 29-31, for the same data and $\Omega/\Omega_0 = 2.5$.

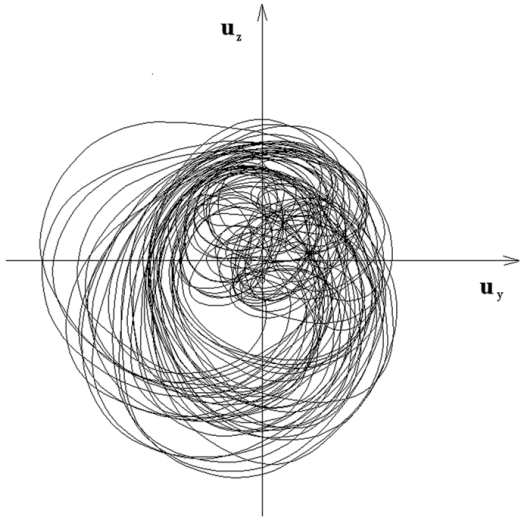

Fig.29 Trajectory of the shaft center for: $s^* = 3$; $f^* = 2.196$; $h^* = 0.2$; $\mu = 0$; $\Omega/\Omega_0 = 2.5$; $\Delta t = 3$ sec

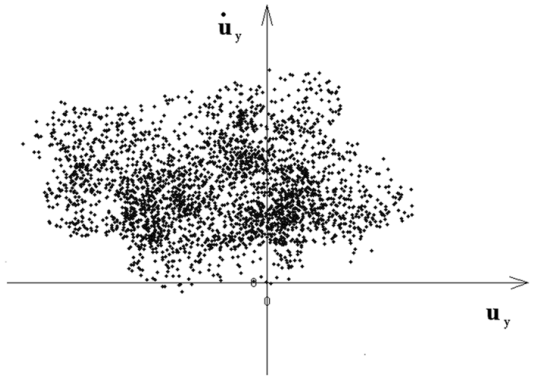

Fig.30 Poincare map for u_y ; $s^* = 3$; $f^* = 2.196$; $h^* = 0.2$; $\mu = 0$; $\Omega/\Omega_0 = 2.5$.

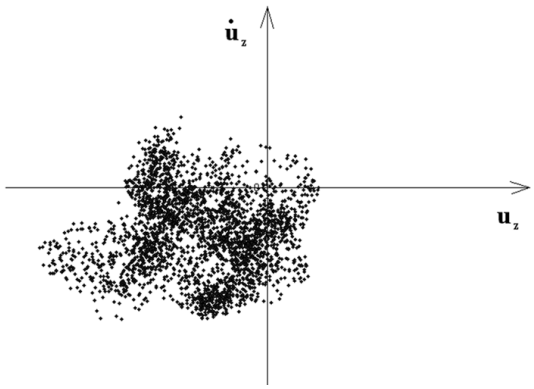

Fig.31 Poincare map for u_z ; $s^* = 3$; $f^* = 2.196$; $h^* = 0.2$; $\mu = 0.$; $\Omega/\Omega_0 = 2.5$.

From pictures in Figs. 29-31 we see that vibrations of the shaft center in this case are probably chaotic.

5. Conclusions

Results of analysis enable us to state that dry friction damper under investigation can effectively limit the shaft vibrations during crossing through the resonance region, but if force f^* is too high, shaft can't left the damper and irregular vibrations may appear. Moderate tangent friction greatly improves the shaft behaviour (Figs 13-20) but if friction is high its influence is not favourable (Figs 21-28).

References

[1] Zienkiewicz O.C., Cheung Y. K. *The finite element method in structural and continum mechanics.* Mc Graw-Hill Publishing Company, London, New-York 1967.

[2] Dżygadło Z., Finite element analysis of natural and forced flexural vibrations of rotor systems. *Jour. Tech. Phys.*, **21**, 1, 1980.

[3] Dżygadło Z., Numerical analysis of flexural vibrations of rotors resting on elastic supports. *Jour. Tech. Phys*., **22**, 4, 1981.

[4] Guckenheimer J., Holmes P. *Nonlinear oscillations, dynamical systems, and bifurcations of vector fields.* Springer-Verlag, New York, Berlin 1983.

[5] Ott E. *Chaos in dynamical systems,* Cambridge University Press, 1993.

[6] Bogusz W., Dżygadło Z., Rogula D., Sobczyk K., Solarz L. *Vibrations.* PWN, Elsevier, Warsaw, Amsterdam 1992.